PAPER

Three regimes of high-voltage breakdown in helium

View the article online for updates and enhancements.

Recent citations

- Plasma-surface interactions
  Trevor Lafleur *et al*

IOP ebooks™

Bringing you innovative digital publishing with leading voices to create your essential collection of books in STEM research.

Start exploring the collection - download the first chapter of every title for free.

Three regimes of high-voltage breakdown in helium

Liang Xu[1,2,4] , **Alexander V Khrabrov**[2], **Igor D Kaganovich**[2] and
Timothy J Sommerer[3]

[1] Department of Modern Physics, University of Science and Technology of China, Hefei, Anhui 230026,
People's Republic of China
[2] Princeton Plasma Physics Laboratory, Princeton, NJ 08543, United States of America
[3] General Electric Global Research, Niskayuna, NY 12309, United States of America

E-mail: hfxuliang@gmail.com and ikaganov@pppl.gov

CrossMark

Abstract

A quasi-analytical model was developed to map out the low-pressure (left-hand) branch of the
Paschen curve at very high voltage when electrons are in the runaway regime and charge
exchange/ionization avalanche sustained by ions and fast neutral atoms becomes important. The
model was applied to helium gas between parallel-plate electrodes, at potentials ranging in
magnitude between 10 and 1000 kV. The respective value of reduced electric field E/n varied in
the range of $50-6000$ kTd (1 kTd $= 10^{-18}$ Vm^2), with reduced density nd (where n is the gas
density and d is the inter-electrode distance) on the order of 10^{20} m^{-2}. Three regimes of the
breakdown have been identified according to the relative share of impact ionization by electrons,
by ions, and by fast neutrals. The analytically derived Paschen curve is compared to those
obtained with a detailed particle-in-cell/Monte Carlo simulation, and also through experimental
measurements (L Xu, A V Khrabrov, I D Kaganovich and T J Sommerer 2017 *Phys. Plasmas* **24**
093511). The model provides accurate predictions for E/n up to $\sim 10^3$ kTd, constrained by
availability and quality of required input data.

1. Introduction

Understanding the mechanism of ionization breakdown in
gases has been a major effort in discharge physics for more
than a century. For parallel-plate DC discharge, the break-
down condition is known as the Paschen law [1], according to
which the breakdown voltage V is a function of the product of
the gas pressure p (or density n) and the electrode separation
d. When the applied voltage is low (say, below 1 kV), the
specific relation between V and pd assumes a simple analy-
tical form. It results from applying a local-field theory to
electron-impact ionization and assuming a constant yield for
ion-induced electron emission [2]. However, under the con-
ditions of high voltage/low pressure on the left-hand branch
of the Paschen curve, additional elementary processes asso-
ciated with fast ions and fast neutrals produced in charge

transfer become necessary for explaining the experimental
data [3–10].

Previously in [11], the authors presented a Paschen curve for
helium, predicted by particle-in-cell/Monte Carlo (PIC/MCC)
simulations of Townsend discharge. The studied range of applied
voltage was 100–1000 kV. It was found, in particular, that
anisotropic scattering of all particle species on the background
neutrals and backscattering of fast neutrals (including ions,
neutralized upon impact) at the cathode surface were essential for
identifying the breakdown state, and had to be accounted for.
The Paschen curve predicted by the kinetic model is double-
valued, with $V(pd)$ having a turning point at approximately
300 kV. This feature indicates an essential role of heavy species
(ions and fast neutrals). It is due to the onset of the runaway
condition, analogously to the violation of locality for electrons at
much lower voltage (kilovolt range in the case of helium). Direct
particle simulation, with adequate models and input data for gas-
phase and surface interactions, allows predicting the properties of

---

[4] Author to whom any correspondence should be addressed.

high-voltage discharge with minimal assumptions. At the same time, it would be of advantage to have a reduced model for which much of the analysis could be carried out analytically. Such a model would provide basic insight into the nature of the process, facilitating both experimental work and verification of the kinetic numerical model.

In theoretical models of gas breakdown, most authors [12–14] only consider the electron-impact ionization source, and the emission of secondary electrons from the cathode due to bombardment by ions, photons, and metastable atoms. This is generally sufficient for *E/n* below 1 kTd. Recently, Loveless and Garner developed a theory that covers the field-emission regime in microscale gaps as well as the classical Paschen law for discharges in a lower range of *E/n* [15]. Efforts to account for the roles of heavy particles, particularly in argon and helium, had been underway for several decades. Jelenković *et al* [16] investigated the Paschen curve in helium for *E/n* in the range 0.3–9 kTd within an electron/ion/fast-neutral model. Local-field equilibrium was assumed for all three particle species, to yield results consistent with experimental data for *E/n* in the range in question. Phelps *et al* [17] established a model for breakdown in argon that accounted for most of the physical processes, also based on local-field equilibrium distributions of electrons, ions and fast neutrals. The Paschen curve predicted by those authors was in excellent agreement with experimental data for *V* < 3 kV, or approximately for *E/n* < 100 kTd. On the other hand, as demonstrated by PIC/MCC simulation [18], in helium electrons undergo a transition to the runaway regime when *E/n* is greater than 850 Td. To address the non-local behavior of electrons in the case of argon, Phelps *et al* [19] applied a 'single beam', or mono-energetic electron beam model and obtained a Paschen curve consistent with experimental results up to 1000 kTd, with a fixed value of ion-induced secondary electron yield $\gamma_i = 0.05$. Early on, Granzow *et al* [20] developed a theoretical model for the low-pressure branch of the Paschen curve for D_2 gas for voltages ranging between 5 and 120 kV. They accounted for charge exchange and ionization by ions and fast neutrals, as well as for backscattering of electrons from the anode, which was found to be important. Macheret and Shneider [10], also investigating breakdown in argon, utilized a 'forward-back' (two-beam) approximation for electron velocity distribution. Those authors also identified the important role of ionization due to accelerated ions and to fast neutrals produced in charge exchange. However, backscattering of ions (which mostly neutralize) and fast neutrals at the cathode surface is essential at *V* > 100 kV and needs to be accounted for in any applicable theory. Also, not much analysis has been done in which energy dependence of charge exchange cross section as well as anisotropy in heavy-particle collisions were both accounted for.

Based on the results of the particle simulations presented in our previous paper [11], the present work aims to develop a realistic and analytical model of gas breakdown in helium for *E/n* on the order of 1000 kTd. Such a model, incorporating electron, ion and fast neutral species, has been formulated to properly describe their interactions with the background gas and with the electrode surfaces. Particular attention has been paid to the significant role of anisotropic scattering experienced by fast atoms and to the particle backscattering at the electrodes, as well as to ionization by fast-neutral impact. The observed double-valued behavior of the Paschen curve, with the turning point at about 200 kV, will be revisited. The specific details of the analytical model are given in section 2 and the results are presented and discussed in section 3. Section 4 summarizes the work.

2. Analytical model

The model accounts for kinetics of positive ions, fast neutral atoms, and electrons in a Townsend discharge in helium at extremely high values of *E/n*. The underlying mechanisms are charge transfer, which controls the velocity distribution of the ions, and the free-fall motion of electrons whose free path exceeds the electrode separation [11]. The high voltage breakdown criterion is defined as the marginal condition where a self-sustained steady state is found, with a balance between total (per unit area) ionization rate and net fluxes of ions (or electrons) through the boundaries.

For the reduced electric field *E/n* on the order of 1000 kTd, velocity distributions of ions transported towards the cathode and of electrons transported towards the anode are strongly peaked near the direction of the electric field. The same applies to fast neutral atoms resulting from charge exchange, due to strongly anisotropic scattering on the background neutrals. The respective velocity distributions will be treated as one-dimensional. Cosine distributions will be assumed for electrons backscattered at the anode and for fast neutrals backscattered at the cathode (meaning half-iso-tropic velocity distributions of the backscattered species in the discharge volume). In the analytical model, the elementary processes responsible for gas-phase ionization are electron-, ion-, and fast-atom impact. Identical to experiments and the PIC/MCC model addressed in our previous paper [11], molybdenum and stainless steel are implemented as electrode materials, respectively, for the cathode and the anode. The accounted surface interactions include ion- and fast-neutral-induced secondary electron emission (SEE) from the cathode, and also fast-neutral backscattering from the cathode. Ion backscattering from the cathode (as neutrals) and fast-neutral backscattering from the anode, which were both accounted for in the particle model [11], will be neglected due to their fluxes being very small compared to the primary (produced by charge transfer) fast-neutral flux collected at the cathode. Photon-induced secondary electron emission, which was verified to be a negligible process in the PIC/MCC model, is also disregarded. Inelastic electron backscattering at the anode plays an important role in gas breakdown [5, 21, 22] and will be accounted for in the effective 'beam' description of the process. We note that all sets of data for energy-dependent cross sections, backscattering coefficients, and
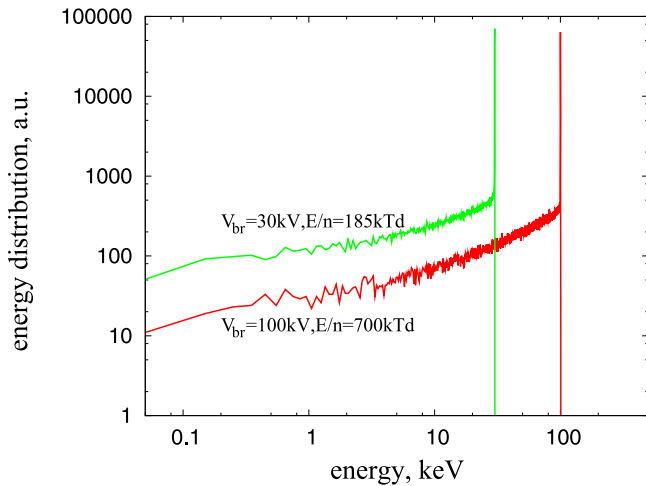
Figure 1. Electron velocity distributions (flux-energy distributions) at the anode found in PIC/MCC simulations at two discharge voltages of 30 kV and 100 kV. It is seen that in both cases electron beams are formed in the gap. The low-energy tails are due to electrons produced by impact ionization of the gas by electrons, ions and fast neutrals. The electrons undergo a free fall and their energy spectrum corresponds to the profile of the ionization rate.

electron emission yields are identical with those in [11], in order to compare the results with those obtained by PIC/MCC simulations. In our model, we use notations $\Gamma_{e,i,a,b}$ to represent the absolute value of the respective flux and the direction from cathode to anode is chosen as positive. Therefore in what follows, in particle balance equations we account for the flux direction by applying an appropriate sign before the positive quantities $\Gamma_{e,i,a,b}$.

2.1. Electron model

For *E/n* in the range of interest for the present study, electrons are in the runaway regime, as already known and verified in particle simulations presented in our preceding work [11]. Figure 1 shows examples of electron velocity distributions (plotted versus energy; without backscattered contribution) at the anode. Electrons emitted from the cathode impact the anode as a ballistic beam. Electrons produced by ionization in the volume are also free-falling, and the shape of their distribution (the tail) is determined by the profile of the ionization rate.

Under the free-fall approximation, the spatial ionization coefficient of electrons $\alpha_{ei}(x)/n$ can be approximated based on a single-beam model [23]:

$$\frac{\alpha_{ei}(x)}{n} = \frac{\int_0^\infty Q_{ei}(\varepsilon)\delta(\varepsilon - eEx)d\varepsilon}{\int_0^\infty \delta(\varepsilon - eEx)d\varepsilon} = Q_{ei}(\varepsilon = eEx), \quad (1)$$

where $Q_{ei}(\varepsilon)$ is the electron-impact ionization cross section and $x = 0$ at the cathode. We follow the terminology of [16, 19] where α/n is called the 'spatial' reaction (e.g., ionization, charge exchange, etc) coefficient. We note that in the extremely

high electric field, electrons backscattered from the anode have an important effect on the electron-ionization coefficient [5, 21, 22, 24]. These electrons become trapped (possibly undergoing repeat reflections) and contribute to ionization as they slow down bouncing off the potential barrier. The particle model [11] allowed for a realistic angular distribution, namely the cosine law, of the backscattered flux, with the backscattering probability $\gamma = 0.028 \exp[1.154(1 - \cos\theta)]$ based on experimental data [25]. In the reduced model, we ignore ionization due to electrons released in the gas. Therefore the ionization by electrons is attributed to the impact of primary (cathode-emitted) electrons and to the electrons backscattered (possibly more than once) at the anode. Because the backscattered electrons are trapped, they do not contribute to the net flux, which is still given by that of the primary electrons. At the same time, the ionization rate due to backscattered electrons will still be proportional to the primary flux and so will be the total electron-impact ionization rate.

In figure 2(a), we show a profile of the spatial ionization coefficient by electrons as deduced from our PIC/MCC simulations, and compare it to that predicted by simulations with no account for electron backscattering. As expected, the difference between the former and the latter increases towards the anode. At the anode surface, it is about a factor of 3. The backscattered electrons that belong to the low-energy portion of the spectrum will be trapped in the vicinity of the anode (especially considering that each successive reflection involves an energy loss). Therefore the profile of the volume ionization coefficient due to backscattered electrons will be inverted relative to that due to the accelerating cathode-emitted primaries. Actually, figure 2(a) indicates that the ionization coefficient in the particle model can be treated as spatially independent over the discharge gap, save in the vicinity of the cathode, where low-energy primary electrons dominate (given that the maximum of electron-impact ionization cross section occurs at energy several times the ionization threshold; about 130 eV for helium). The weakly varying spatial ionization coefficient is also observed at other values of the breakdown voltage, as seen in figure 2(b) where three cases are presented.

If, as discussed above, the electron-ionization reaction coefficient can be reasonably approximated by a constant value in the entire discharge gap, the description of non-local electron kinetics becomes simplified and the ionization coefficient can be treated as effectively 'local'. In figure 3 the constant-value approximations of electron-induced ionization coefficient $\alpha_{ei}/n(E, n)$, obtained in PIC/MCC simulations for breakdown voltage 15 kV $< V_{br} <$ 1000 kV, are plotted versus eV_{br}. This data allows a simple analytical fit which is valid for the voltage range of 10–1000 kV:

$$\frac{\alpha_{ei}(x)}{n} \simeq \frac{\alpha_{ei}}{n}(E, n) = 1.0 \times 10^{-22} \times [0.436 + 1.468$$
$$\times 10^5/(eV_{br} - 1206.8)], \qquad (2)$$
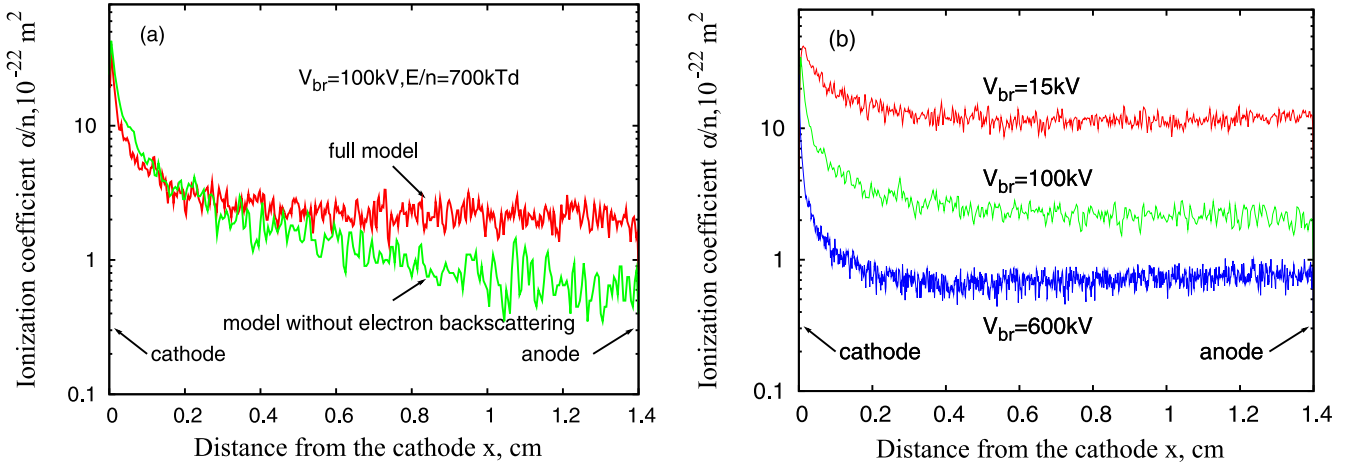
Figure 2. Ionization coefficients α/n for electrons found in PIC/MCC simulations [11]: (a) spatial ionization coefficients obtained in the full model and the model without electron backscattering, for breakdown voltage of 100 kV, and (b) spatial ionization coefficients obtained for breakdown voltages of 15 kV, 100 kV, and 600 kV.
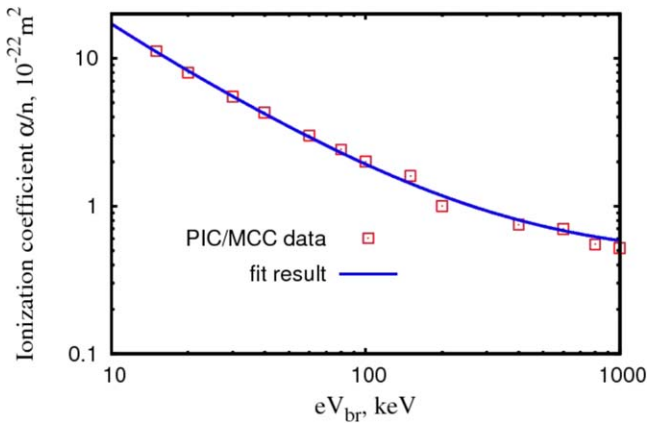
Figure 3. Analytical fit for the ionization coefficient versus eV_{br} with account for both primary and backscattered electron fluxes.

where V_{br} is in volts. The value of α_{ei} can be now used in the fluid equation for electron flux in the steady state:

$$\frac{d\Gamma_e(x)}{dx} = \alpha_{ei}(E, n)\Gamma_e(x) + \alpha_{ii}(E/n)\Gamma_i(x) + \alpha_{ai}(E/n)$$
$$\times \Gamma_a(x) + \alpha_{bi}(E/n)\Gamma_b(x),$$

$$(3)$$

where $\Gamma_e(x), \Gamma_i(x), \Gamma_a(x), \Gamma_b(x)$, respectively, are the particle fluxes of electrons, ions, primary fast atoms, and backscattered fast atoms. Therefore the electron flux is increasing toward the anode due to the combined ionization processes. The quantities $\alpha_{ii}/n(E/n), \alpha_{ai}/n(E/n), \alpha_{bi}/n(E/n)$ are ion-, fast-neutral-, and backscattered fast-neutral-impact ionization coefficients in helium. The values of coefficients α_x/n for ions and fast atoms are discussed in appendix A. Electron-impact ionization of helium is the only process with a significant contribution when $E/n < 4.3$ kTd [9]. Other contributions to the electron particle balance, e.g. electron–ion recombination or associative ionization, can be neglected for the low-current Townsend discharge.

2.2. Ion model

The model for He$^+$ ions is based on local equilibrium distribution governed by charge transfer [19, 26], i.e. it is being assumed that the free path λ_{cx} for charge transfer is much smaller than the discharge gap. This assumption was verified in the PIC/MCC study of breakdown in helium [11] according to which λ_{cx} is one order smaller than the discharge gap even in the 1000 kTd regime. We note that charge exchange collisions present a friction mechanism in the momentum transfer equation, but do not affect the flux continuity. In addition, the net current in a steady state should be conserved:

$$\Gamma_e(x) + \Gamma_i(x) = \text{constant}. \tag{4}$$

Therefore due to the ionization of the gas by electrons, ions and fast neutrals, the ion flux increases towards the cathode and obeys the following equation:

$$\frac{d\Gamma_i(x)}{dx} = -\frac{d\Gamma_e(x)}{dx} = -\alpha_{ei}(E, n)\Gamma_e(x) - \alpha_{ii}(E/n)\Gamma_i(x)$$
$$- \alpha_{ai}(E/n)\Gamma_a(x) - \alpha_{bi}(E/n)\Gamma_b(x).$$

$$(5)$$

Accounting only for charge transfer, the dominant collision type for ions, we solve the resulting steady-state Boltzmann equation. The charge exchange cross section approximates as $\sigma_{cx}(\varepsilon) = [A - B \ln \varepsilon]^2 \times \sigma_0$, where $A = 5.282$, $B = 0.294$, $\sigma_0 = 10^{-20}$ m^2 and energy ε is in eV. The energy distribution function is obtained by solving the Boltzmann transport equation using the Bhatnagar–Gross–Krook (BGK) approximation [27] based on the assumption that the charge exchange is the dominant ion–neutral collisional process.

$$f(\varepsilon) = C \exp\left[-\varepsilon \frac{A^2 + B^2 \ln^2 \varepsilon - 2(AB + B^2)(\ln \varepsilon - 1)}{E/n\sigma_0}\right]$$

$$(6)$$
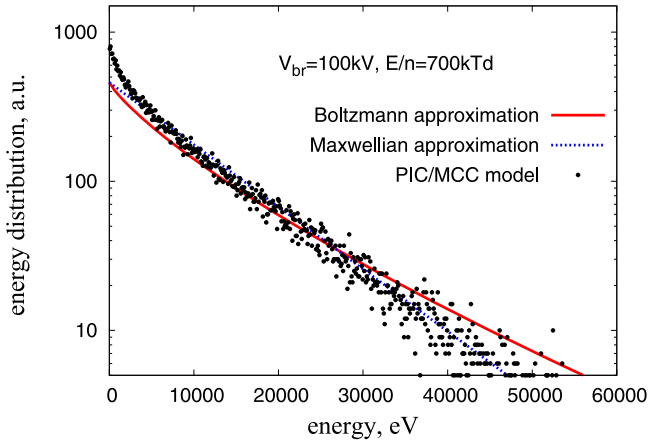
Figure 4. Ion velocity distribution function, versus energy, measured at the cathode in PIC/MCC simulations [11] at the breakdown voltage of 100 kV, compared with the Maxwellian fit (7) and with the local-approximation solution (6) based on the Boltzmann equation. It is interesting to observe that the Maxwellian approximation shows good agreement with the PIC/MCC result over much of the energy range, except at low energies below 3 keV, whereas the local Boltzmann solution predicts a hotter tail. This phenomenon is attributed to 'loading' of the distribution with freshly produced slow ions. The detailed interpretation will be addressed in our future work.

where C is the normalization factor defined by the flux. We note, however, that the Boltzmann solution (local approximation) shows large deviation from the ion spectrum observed in PIC/MCC simulations, as seen in figure 4 for the case of $V_{br} = 100$ kV. The Boltzmann solution predicts a 'hotter' tail. This indicates that ionization frequency can be comparable to charge exchange frequency, to result in a large number of slow ions released in the ionizing collisions. This effect will be studied in future work. Another option is to adopt a one-dimensional Maxwellian distribution with 'temperature' T_i on the order of $eE\lambda_{cx}$ to approximate the ion velocity distribution as $f_i(\varepsilon) = C' \exp(-\varepsilon/T_i)$, where C' is again the defined by the flux. This approach (Maxwellian approximation) was adopted by Phelps *et al* [28] for high values of *E/n*. The empirical fit for ion temperature versus *E/n* is based on experimental data:

$$T_i = 4[(E/n)/1000]^{1.2}, \qquad (7)$$

where *E/n* is in Td and T_i is in eV. In figure 4, the above approximation is also compared to the ion energy distribution function yielded by PIC/MCC model for a breakdown voltage of 100 kV. It is found that the Maxwellian approximation shows good agreement with the PIC/MCC result, except at very low energies (<3 keV). The deviation at low energies does not cause a big error in the total ionization rate, which is mostly determined by fast neutrals, because in the *E/n* regime of interest here, high-energy fast neutrals produced via charge transfer by high-energy ions contribute the most to ionizing the gas. This is demonstrated in figure 10 and makes the Maxwellian–IVDF approximation a reasonable one for our purposes.

Next, the charge-transfer coefficient α_{ct}/n and the ionization coefficient α_{ii}/n for He$^+$ in neutral helium are plotted versus the reduced electric field *E/n* in figure 5. These
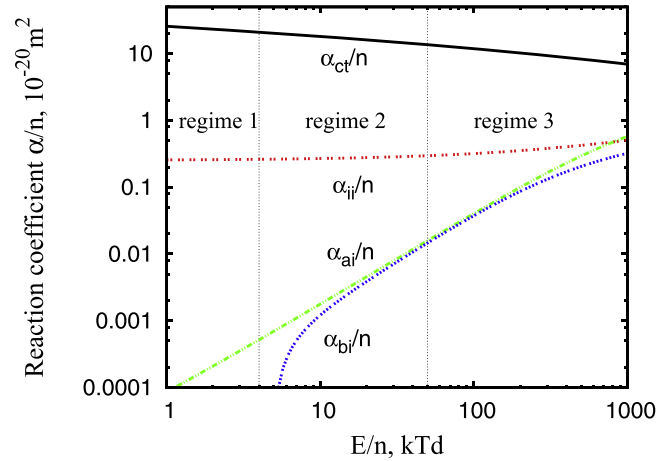
Figure 5. Reaction coefficients for He$^+$ and fast helium atoms (primary and backscattered) in background helium gas. Only those reactions that are essential to creating an ion–fast-neutral–ion avalanche are taken into account. For ions, only charge transfer (α_{ct}/n) and ionization (α_{ii}/n) processes are considered. For primary and backscattered fast neutrals, only the ionization reactions (α_{ai}/n or α_{bi}/n) are taken into account. The values of the coefficients are discussed in appendix A. The regimes are defined in table 1.

coefficients are obtained by flux-averaging the respective cross sections over the one-dimensional ion distribution and the details are given in appendix A. The same cross sections as adopted by the authors in [11] are utilized in the present work.

Regarding the surface interactions, the analytical model accounts for SEE induced by both ions and fast neutrals. Therefore the electron flux leaving the cathode can be expressed as following:

$$\Gamma_e(0) = \gamma_i(E/n)\Gamma_i(0) + \gamma_f(E/n)\Gamma_a(0), \qquad (8)$$

where γ_i and γ_f are the *E/n*-dependent secondary yields induced, respectively, by ions and by fast neutrals. The yield coefficients that relate net fluxes are obtained by averaging the respective energy-dependent SEE yields over the ion and corresponding primary fast-atom distributions. The resulting yield coefficients (surface-reaction rates) are discussed in appendix A and plotted in figure 6.

The boundary condition for ions at the anode states that there are no accelerated ions; the same applies to fast neutrals:

$$\Gamma_i(d) = \Gamma_a(d) = 0. \qquad (9)$$

Ions emitted from the anode due to electron bombardment are ignored, as is the tertiary flux of backscattered fast neutrals.

2.3. Fast neutral atom model

Fast atoms are generated primarily via charge transfer and therefore their velocity distribution is governed by that of the projectile He$^+$ ions [19, 26]. In studies of high-voltage discharges, e.g. [10, 16, 17], the usual assumption has been that any elastic or inelastic collision of a fast neutral with a background atom of equal mass would result in a loss of that fast neutral, by reducing its energy below the threshold of excitation or ionization. However, the situation is different
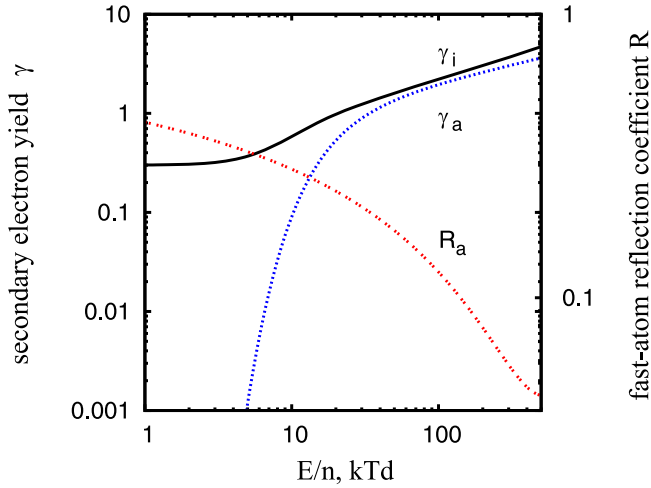
Figure 6. Surface interaction coefficients: secondary electron yield due to ions (γ_i) and to fast atoms (γ_a), and fast-atom backscattering coefficient (R_a). The values of these coefficients are considered in appendix A.

with anisotropic scattering, which occurs at ion/atom energies corresponding to high values of *E/n*. Energy loss by fast atoms can be negligible in elastic and excitation collisions due to small scattering angles. The main loss channel for fast neutrals will be through ionization, because stripping of the projectile and ionization of the target occur with equal probability. Therefore the equation for the fast neutral flux traveling towards the cathode (in the negative direction) can be written as follows:

$$\frac{d\Gamma_a(x)}{dx} = -\alpha_{ct}(E/n)\Gamma_i(x) + \frac{1}{2}\alpha_{ai}(E/n)\Gamma_a(x). \quad (10)$$

The ionization coefficient α_{ai}/n in equation (10) is obtained by averaging the neutral-impact-ionization cross section $Q_{ai}(\varepsilon)$ over the fast-neutral energy distribution. For this purpose, assuming the first term in (10) dominates over the second, the first approximation for the neutral distribution will suffice, namely $f_a(\varepsilon) \propto Q_{ct}(\varepsilon)f_i(\varepsilon)$. The result is

$$\frac{\alpha_{ai}}{n}\left(\frac{E}{n}\right) = \frac{\int_0^\infty Q_{ai}(\varepsilon)f_a(\varepsilon)d\varepsilon}{\int_0^\infty f_a(\varepsilon)d\varepsilon} = \frac{\int_0^\infty Q_{ct}(\varepsilon)Q_{ai}(\varepsilon)f_i(\varepsilon)d\varepsilon}{\int_0^\infty Q_{ct}(\varepsilon)f_i(\varepsilon)d\varepsilon}. \quad (11)$$

The slowly decreasing $Q_{ct}(\varepsilon)$ results in a 'cooler' distribution of fast atoms versus that of the ions. At the cathode, primary fast neutrals will be backscattered and travel freely against the electric field, which is essential for initiating the heavy-species ionization avalanche in the vicinity of the anode. As is the case for primary fast atoms, stripping is the prevailing elimination mechanism for the backscattered neutrals. Therefore for the backscattered fast-atom flux, dubbed Γ_b, we have

$$\frac{d\Gamma_b(x)}{dx} = -\frac{1}{2}\alpha_{bi}(E/n)\Gamma_b(x), \quad (12)$$

where α_{bi}/n is the flux-averaged ionization coefficient for backscattered fast neutrals, calculated by averaging the fast-atom

ionization cross section $Q_{ai}(\varepsilon)$ over the backscattered fast-atom energy distribution $f_b(\varepsilon) \propto R_N(\varepsilon)f_a(\varepsilon) \propto Q_{ct}(\varepsilon)R_N(\varepsilon)f_i(\varepsilon)$. Because a good model for the energy spectrum of backscattered flux is not available, the energy of a reflected atom is calculated simply as $\varepsilon' = \varepsilon \frac{R_E(\varepsilon)}{R_N(\varepsilon)}$, where $R_N(\varepsilon)$ and $R_E(\varepsilon)$ are, respectively, the particle flux and the energy flux reflection coefficients for the primary atom energy ε. Also, a cosine angular distribution is adopted for the backscattered flux, the same as in [11]. The resulting expression for backscattered-fast-neutral ionization coefficient is

$$\frac{\alpha_{bi}}{n}\left(\frac{E}{n}\right) = \frac{\int_0^\infty R_N(\varepsilon)Q_{ct}(\varepsilon)Q_{ai}(\varepsilon')f_i(\varepsilon)d\varepsilon}{\int_0^\infty Q_{ct}(\varepsilon)R_N(\varepsilon)f_i(\varepsilon)d\varepsilon}$$
$$\times \frac{\int_0^{\pi/2} \cos\theta \sin\theta d\theta}{\int_0^{\pi/2} \cos^2\theta \sin\theta d\theta}. \quad (13)$$

where the first factor on the right is similar to equation (11) and the second factor is 3/2. The calculated α_{bi}/n is plotted in figure 5. It is seen that even with account for angular distribution, values of α_{bi}/n are always smaller than those of α_{ai}/n, indicating the importance of energy loss in inelastic backscattering.

Next, to formulate the cathode boundary condition for the fast neutral flux, we need an expression for the reflection coefficient $R_a(E/n)$. It is obtained by averaging the energy-dependent particle backscattering coefficient $R_N(\varepsilon)$ over the primary fast-atom distribution $f_a(\varepsilon)$:

$$R_a\left(\frac{E}{n}\right) = \frac{\int_0^\infty Q_{ct}(\varepsilon)R_N(\varepsilon)f_i(\varepsilon)d\varepsilon}{\int_0^\infty Q_{ct}(\varepsilon)f_i(\varepsilon)d\varepsilon}. \quad (14)$$

This coefficient is plotted in figure 6 and its calculation is presented in appendix A. Therefore the backscattered fast neutral flux at the cathode is given by

$$\Gamma_b(0) = R_a\Gamma_a(0). \quad (15)$$

Here, we note that in the present model the ions neutralized and then backscattered as neutrals at the cathode are neglected, due to their flux being much smaller than the primary fast-neutral flux. The fast atoms repeatedly backscattered at the anode are likewise neglected, because their flux is on the order of $R_a^2 \ll 1$ and their energy spectrum also degrades upon successive reflections.

3. Results and discussion

3.1. The physics of ionization avalanche

To gain insight into how the avalanche is sustained in very high electric field, we consider spatial profiles of particle fluxes predicted by the analytical model for the breakdown state. Figure 7 shows the calculated fluxes of electrons, ions and fast neutrals, compared with those obtained in a PIC/MCC simulation of a breakdown state for $V_{br} = 100\,kV$,
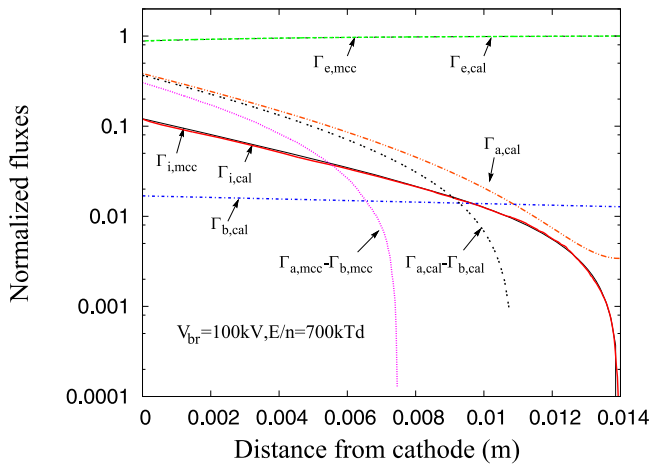
Figure 7. Spatial profiles of normalized fluxes of electrons $\Gamma_{e,cal}$, He^+ ions $\Gamma_{i,cal}$, primary fast atoms $\Gamma_{a,cal}$, and reflected fast atoms $\Gamma_{b,cal}$, compared to the corresponding fluxes $\Gamma_{e,mcc}$, $\Gamma_{i,mcc}$ and ($\Gamma_{a,mcc} - \Gamma_{b,mcc}$) obtained with the PIC/MCC model [11] at a breakdown voltage of 100 kV. Electron flux and ion flux are seen to be in excellent agreement between the analytical model and the PIC/MCC model, while the net fast-atom flux ($\Gamma_{a,cal} - \Gamma_{b,cal}$) does not agree with the PIC/MCC result ($\Gamma_{a,mcc} - \Gamma_{b,mcc}$). The discrepancy is due to the fast-neutral species definition in our PIC/MCC model: only those atoms with energies above 200 eV are tracked as 'fast neutrals'. The particle flux calculation is discussed in appendix B.

with corresponding gas density $n = 1.018 \times 10^{22} \, m^{-3}$. The particle fluxes are normalized to the constant total flux $\Gamma_t = \Gamma_i + \Gamma_e$ and the calculation details are given in appendix B. As seen in figure 7, the calculated electron and ion fluxes are in excellent agreement with the particle simulation results. The relative change in the electron flux over the gap is small because the secondary yield at the cathode due to energetic neutral flux (about 10) is much higher than the multiplication factor (which is correspondingly about 1.1). We note that in both analytical and numerical PIC/MCC models, the net flux of fast neutrals ($\Gamma_a - \Gamma_b$) is negative within some distance of the anode, because $\Gamma_a(d) = 0$ in the former and $\Gamma_a(d) = R\,\Gamma_b(d)$ in the latter, with $R \ll 1$. The deviation between net fast-neutral fluxes ($\Gamma_{a,cal} - \Gamma_{b,cal}$) of the reduced model and ($\Gamma_{a,mcc} - \Gamma_{b,mcc}$) of the particle model is, for the most part, due to low-energy cut-off applied to fast neutral species in the PIC/MCC code. The cut-off is at an energy of 200 eV where the ionization frequency becomes negligible.

In order to identify the roles of individual particle species in sustaining the charge multiplication avalanche, in figure 8 we plot the profiles of gas ionization rates due to electrons, ions, primary fast atoms, and backscattered fast atoms for the case when the breakdown voltage is 100 kV. Note that the ionization rate is, again, normalized by the net charge flux ($\Gamma_e + \Gamma_i$). It is clearly seen that primary fast neutrals make the largest contribution to the ionization rate, and it increases from the anode towards the cathode as the flux of fast neutrals multiplies. Near the cathode, the electron-impact ionization rate is much smaller than that due to fast atoms and to ions, but the opposite is true in the vicinity of the anode. On the whole, in the total ionization rate integrated over the gap, the
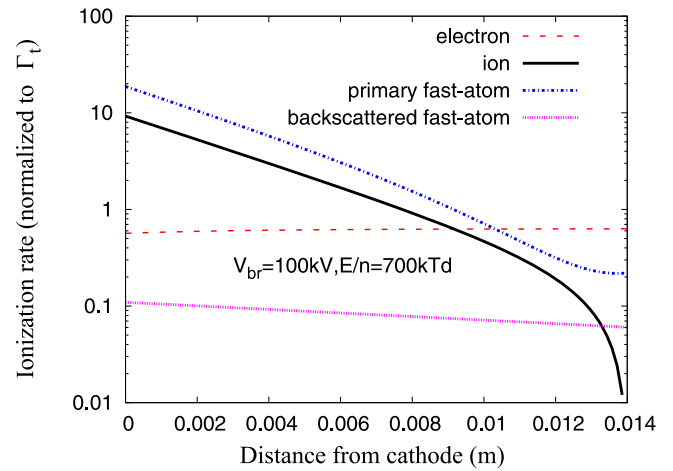
Figure 8. Ionization rates due to impact by electrons, ions, primary fast atoms, and backscattered fast atoms calculated in the reduced analytical model. Their profiles are determined by the respective fluxes. Overall, the fast-atom contribution to net ionization is the largest and electrons contribute about the same as ions.

share of electrons among the three species is only 22% and that of fast neutrals (primary + backscattered) is as high as 57%.

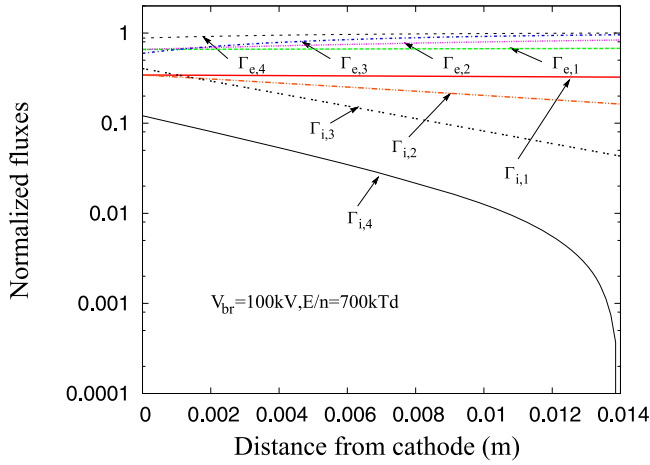### 3.2. Three regimes of breakdown discharge

The structure of the breakdown discharge changes in accordance with the value of the reduced electric field E/n, which controls the volume-reaction and surface-reaction (electron emission and backscattering) rates of each particle species. Therefore it is of interest to identify distinct regimes of the breakdown and discuss transitions from one to another. Presently, we introduce three such regimes, called (1) 'the electron regime', (2) 'the ion regime', and (3) 'the fast-atom regime'. The ordering corresponds to increasing E/n. Based on our model and previous work on electrical breakdown in helium, these regimes can be distinguished qualitatively according to the importance of gas ionization by each of the respective particle species. In regime 1, identified for helium as $E/n < 4$ kTd, the discharge is sustained only by electrons, because fast-neutral energies and ion energies are both below ionization thresholds. In regime 2, identified as 4 kTd $< E/n < 50$ kTd, the ion-species contribution to the gas-phase ionization prevails over those of electrons and of fast neutrals. In regime 3, identified as $E/n > 50$ kTd, ionization by all three particle species is important. In table 1 we identify the roles of various elementary physical processes under the three regimes listed above. In fact, the corresponding portions of the Paschen curve can be adequately described by models (presented below) obtained by further truncating the reduced analytical model under study, although for regimes 1 and 2, local-field model for electrons [2, 16] should be applied instead of the free-flight model considered presently.

In order to highlight the differences between three different regimes 1, 2, and 3, we introduce three reduced models, identified with the aid of table 1. In each of these models, we disable those elementary processes of the base model which

8

Table 1. Gas-phase elementary processes and particle–surface interactions accounted for in reduced models under different regimes of breakdown.

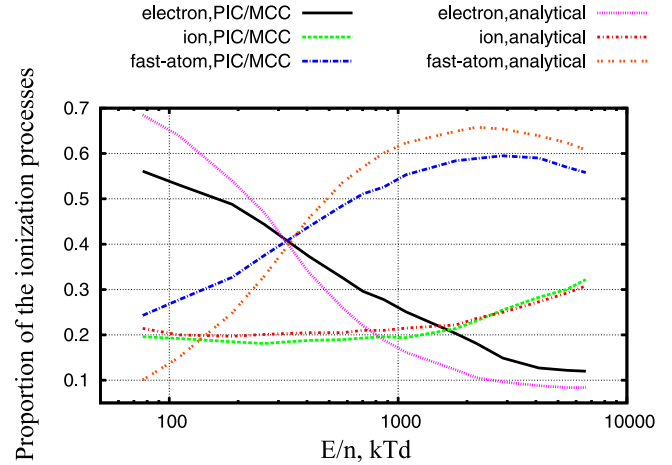|	Reaction					
Regime	Electron ionization	Ion ionization	Fast-atom ionization	Ion-induced electron emission	Fast-atom induced electron emission	Fast-atom backscattering
Regime 1 (model 1)	✓			✓		
Regime 2 (model 2)	✓	✓		✓	(depends on cathode material)	
Regime 3 (model 3)	✓	✓	✓	✓	✓	
Regime 3 (model 4)	✓	✓	✓	✓	✓	✓

Figure 9. Calculated profiles of normalized fluxes of electrons, $\Gamma_{e,1}$, $\Gamma_{e,2}$, $\Gamma_{e,3}$, and $\Gamma_{e,4}$, and ions, $\Gamma_{i,1}$, $\Gamma_{i,2}$, $\Gamma_{i,3}$, and $\Gamma_{i,4}$ for breakdown models 1, 2, 3, and 4 specified in the text, for the case in which the breakdown potential is 100 kV. The solutions of the truncated models 1, 2, 3 successively become closer to that of the complete model 4. The difference between model 3 and model 4 indicates that fast-atom backscattering is crucial in high-voltage breakdown. The particle flux calculation is discussed in detail in appendix B.

Figure 10. Fractions of gap-integrated ionization rate due to electron-impact ionization, ion-impact ionization, and fast-atom-impact ionization.

can be neglected. The complete (base) model is labeled 'model 4'. We note that in model 3, the process of fast-neutral backscattering is also neglected, to observe (and compare with model 4) the effect of such an assumption, commonly used in the literature. Therefore the reduced models can be characterized as follows.

1. First reduced model: $\alpha_{ii} = \alpha_{ai} = \gamma_a = R_a = 0$.
2. Second reduced model: $\alpha_{ai} = \gamma_a = R_a = 0$.
3. Third reduced model: $R_a = 0$.
4. Non-truncated model.

Figure 9 shows normalized particle fluxes of models 1, 2, 3 and 4 for the gas pressure at which the breakdown voltage is 100 kV. The calculations of electron and ion fluxes are discussed in detail in appendix B. Note that in all cases, the electron-ionization coefficient α_{ei}/n of section 2.1 is still utilized instead of the value obtained through local-field model. This introduces a lower limit on the discharge voltage to which the description applies. From figure 9, it is seen that the solutions obtained with models 1, 2, and 3 differ from that of model 4, and become successively closer to it. This observation illustrates the importance of ionization by ion and fast-neutral impact. In addition, for model 3, the absence of fast-atom reflection from the cathode results not only in reduced ionization compared to model 4, but also the disappearance of the applicable self-organization mechanism of the discharge [11]. The backscattered fast atoms ionize the gas in the gap, and the resulting ions undergo multiple cycles of acceleration and charge exchange to re-generate the primary fast atoms beam that impinge upon the cathode. This self-organization mechanism is essential for sustaining the discharge current and initiating the breakdown, even without electron-ionization impact in the 100–1000 kV range [11].

For regime 3 (the fast-neutral regime) of interest in this work, in figure 10 we visualize the relative shares of impact ionization processes by different species (electrons, ions, and fast neutrals) in the net ionization rate. The results produced by the analytical model are compared with those of with PIC/MCC simulations. Good agreement is obtained between the two sets of results. It is seen that in regime 3, electron-impact ionization is no longer the prevailing contribution to the production of ion–electron pairs and decreases monotonically with increasing E/n. The share of ion-impact ionization increases from 18% to 30% over the investigated range of E/n. The share of fast-atom impact ionization increases more sharply and becomes the largest when E/n exceeds 300 kTd.

3.3. Analytical solution for the breakdown threshold

The breakdown threshold is defined as a condition for existence of a non-trivial solution for the set of time-independent particle balance equations (3), (5), (10), and (12) (refer to model 4 in table 1). Such a condition corresponds to a functional dependence between $E/n = V/nd$ and nd, i.e. the Paschen curve. The linear equations (3), (5), (10) and (12) are solved subject to appropriate boundary conditions, given by equations (8), (9), and (15). The resulting compatibility condition (an implicit equation for the Paschen curve), necessary for a non-trivial solution, can be expressed as follows:
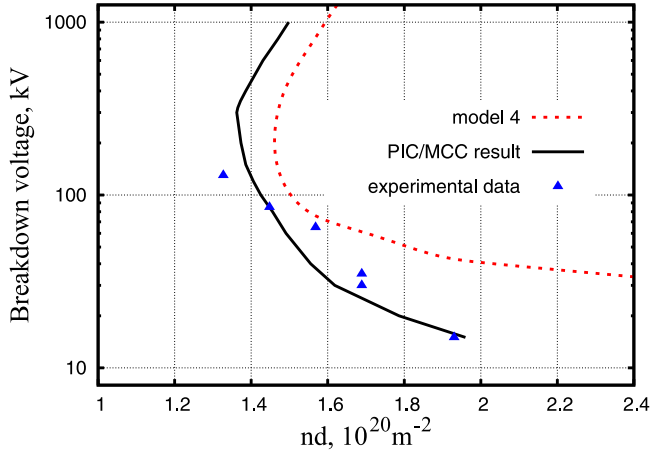
$$A \exp(\lambda_1 d) + B \exp(\lambda_2 d) + C \exp(\lambda_3 d) + D$$
$$\times \exp[(\lambda_1 + \lambda_2)d] + E \exp[(\lambda_1 + \lambda_3)d] + F$$
$$\times \exp[(\lambda_2 + \lambda_3)d] = 0, \tag{16}$$

where $A = [R_a (1 + \gamma_i) (N-Q) - \beta (1 + \gamma_i + N\gamma_a)] (S - PM)$, $B = [R_a (1 + \gamma_i) (M + Q) + \beta (1 + \gamma_i + M\gamma_a)] (S - PN)$,

$$C = (M - N)(1 + \gamma_i)(S - PQ)R_a,$$

$$D = [(QR_a + \beta)(1 + P\gamma_i + S\gamma_a) - S(1 + \gamma_i + Q\gamma_a)]$$
$$(N - M),$$

$$E = [-NR_a(1 + P\gamma_i + S\gamma_a) + S(1 + \gamma_i + N\gamma_a)](Q - M),$$

Figure 11. Paschen curves based on the present analytical calculation being compared with PIC/MCC simulation result, and with experimental data (the latter two from [11]). The experiment covers the range between 15 kV and 130 kV. The analytical model and the PIC/MCC simulation both predict a turning point above 200 kV, i.e., double-valued behavior.

$$F = [MR_{\mathrm{a}}(1 + P\gamma_{\mathrm{i}} + S\gamma_{\mathrm{a}}) - S(1 + \gamma_{\mathrm{i}} + M\gamma_{\mathrm{a}})](Q - N),$$

$$M = \frac{\alpha_{ct}}{\alpha_{\mathrm{ai}}/2 - \lambda_{\mathrm{l}}}, \quad N = \frac{\alpha_{\mathrm{ct}}}{\alpha_{\mathrm{ai}}/2 - \lambda_2}, \quad Q = \frac{\alpha_{\mathrm{ct}}}{\alpha_{\mathrm{ai}}/2 - \lambda_3},$$

$$P = \frac{\alpha_{\mathrm{ei}}}{\alpha_{\mathrm{ii}} + 2\alpha_{\mathrm{ct}}}, \quad S = \frac{2\alpha_{\mathrm{ei}}\alpha_{\mathrm{ct}}}{\alpha_{\mathrm{ai}}(\alpha_{\mathrm{ii}} + 2\alpha_{\mathrm{ct}})}, \quad \text{and} \quad \beta = -\frac{\alpha_{\mathrm{ei}}}{\alpha_{\mathrm{bi}}} +$$

$$\frac{\alpha_{\mathrm{ii}}}{\alpha_{\mathrm{bi}}} + \frac{\lambda_3}{\alpha_{\mathrm{bi}}} + \frac{\alpha_{\mathrm{ai}}\alpha_{\mathrm{ct}}}{(\alpha_{\mathrm{ai}}/2 - \lambda_3)\alpha_{\mathrm{bi}}}.$$ The four eigenvalues of the matrix corresponding to (3), (5), (10) and (12) are 0 and also $\lambda_{\mathrm{l},2} = \frac{1}{2}[(\alpha_{\mathrm{ei}} + \alpha_{\mathrm{ai}}/2 - \alpha_{\mathrm{ii}}) \pm \sqrt{(\alpha_{\mathrm{ei}} + \alpha_{\mathrm{ai}}/2 - \alpha_{\mathrm{ii}})^2 + 4(\alpha_{\mathrm{ai}}\alpha_{\mathrm{ct}} + \alpha_{\mathrm{ai}}\alpha_{\mathrm{ii}}/2 - \alpha_{\mathrm{ei}}\alpha_{\mathrm{ai}}/2)},$ $\lambda_3 = -\alpha_{\mathrm{bi}}/2$

The Paschen curve defined by equation (16) is shown in figure 11 for 10 kV < V < 1000 kV, alongside the PIC/MCC and experimental results of [11]. The three sets of data are consistent with each other. The analytical model predicts a turning point at about 200 kV, versus the value 300 kV predicted by the present PIC/MCC model. The respective values of reduced pressure differ by less than 10% when voltage is larger than 50 kV. The discrepancy between the present analytical result and the PIC/MCC model is due to several approximations, e.g., assuming local equilibrium energy distribution of the ions (which is not actually present within several free-path lengths of anode) as well as neglecting ion backscattering at the cathode and fast-neutral backscattering at the anode. Below 50 kV, the large discrepancy observed between the reduced model and the PIC/MCC result indicates that the high-voltage electron model fails to adequately describe the electron velocity distribution.

3.4. Role of fast-neutral gas ionization and backscattering

To evaluate the significance of fast-neutral backscattering at the electrodes, we obtained the Paschen curve for a model in which this process was disabled. The results are shown in figure 12. As expected, the absence of backscattered flux causes the Paschen curve to shift to the right. Reducing the
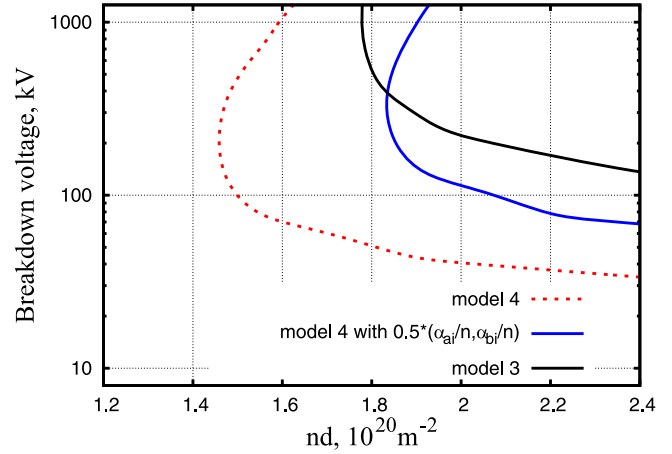
Figure 12. Comparison of Paschen curves between the full model (model 4), model 4 with the fast-atom-impact ionization coefficient reduced by a factor of 2 (for both primary and cathode-backscattered fluxes), and the model with no fast-neutral backscattering at the cathode (model 3). Both modifications to the model cause the Paschen curve to shift strongly to the right, which is indicative of the importance of fast-neutral-impact ionization and backscattering.

backscattering coefficient to zero obviously has a more pronounced effect at lower voltage. This is attributed to the decrease of the backscattering yield with increasing projectile energy. This comparison clearly emphasizes the importance of fast-atom backscattering at the cathode for sustaining a Townsend discharge at high voltage.

We also carried out another calculation, with the fast-atom-impact ionization coefficient reduced by half, for all values of *E/n*, versus the actual value based on cross-section data. It was done in order to investigate the effect of the fast-atom-impact ionization. The large deviation of the resulting Paschen curve, also shown in figure 12, from that based on the unaltered model demonstrates the fast-atom-impact ionization to be essential at high voltage.

3.5. Effect of fast-atom stripping losses

With strongly anisotropic (i.e. peaked near 0° and 180° in the center-of-mass frame) neutral/neutral scattering built into the model, whenever a fast neutral atom undergoes stripping in an ionizing collision, the target atom remains slow and therefore a fast neutral is lost with a probability of 1/2. To show the importance of this effect, we created another artificial case by eliminating the respective loss term in equations (10) and (12) so that only the background atoms ionize. The resulting Paschen curve is shown in figure 13. It gives much lower values of reduced pressure for a given breakdown voltage over the entire range. The extra ionization in the artificial model is due to additional fast neutrals.

3.6. Ion–neutral runaway and the turning point on the predicted Paschen curve
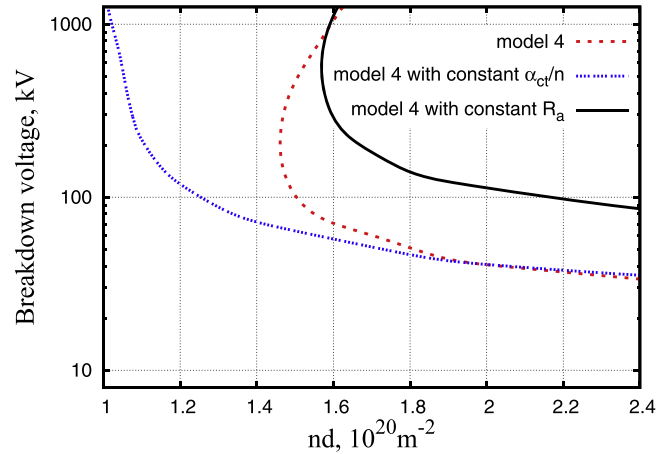
The physical mechanism behind the presence of the turning point is that the velocity distributions of the ionizing species,
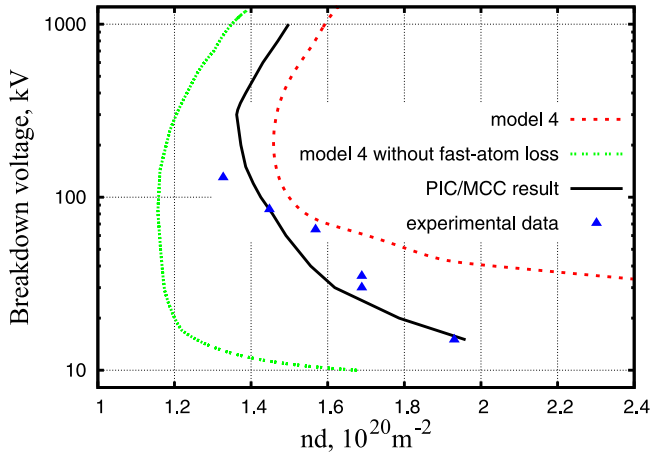
Figure 13. Paschen curves obtained with the full model (model 4) and in the artificial case without stripping loss of fast-atom, along with the PIC/MCC prediction and experimental results.

Figure 14. Paschen curves obtained in two numerical experiments with artificial input data: one with constant charge-transfer cross section $\alpha_{ct}/n = 1.0 \times 10^{-19}\,\mathrm{m}^{-2}$, and another with constant back-scattering coefficient $R_a = 0.05$ for fast neutrals at the cathode. The unaltered (model 4) result is also shown for comparison.

in this case ions and fast neutrals, undergo a transition to the runaway regime. This phenomenon has already been observed for electrons, in which case it occurs at the breakdown voltage in the range of several kV [9]. Experimentally, such turning points have been observed for helium and mercury [9, 29], and to a lesser extent for neon. Basically, the multiplication length becomes comparable with the electrode spacing and increases monotonically with respect to the applied voltage. Because this length has to fit into the gap, the *nd* value now needs to increase with voltage to have sufficient ionization. We note that the multiplication length in the regime in question can be estimated as $1/\sqrt{\alpha_{ct}\alpha_{ai}}$, based on the expressions for the eigenvalues given above.

The decrease in charge-transfer coefficient α_{ct}/n with increasing *E/n* is the primary cause of the runaway transition. To verify this, we performed yet another numerical experiment, with a constant (not depending on *E/n*) charge-transfer reaction coefficient $\alpha_{ct}/n = 1.0 \times 10^{-19}\,\mathrm{m}^{-2}$. The comparison with an unaltered Paschen curve is presented in figure 14. The turning point disappears for the model with constant charge-transfer reaction coefficient. The decrease in the fast-atom reflection coefficient with increasing *E/n* (plotted in figure 6) also affects the onset of the runaway regime. The role of this parameter is rather similar to that of secondary electron yield at lower voltage, although ion–neutral ionization avalanches initiated by backscattered fast atoms actually propagate towards the cathode. The result of a calculation with a constant value of the fast-atom reflection coefficient, set at $R_a = 0.05$, is also shown in figure 14. The turning point in this example is at about $V_{br} = 600\,\mathrm{kV}$, much higher than 200 kV predicted by the unaltered model. With the reflection coefficient falling off at high *E/n*, the discharge gap-to-multiplication-length ratio needs to increase (while the multiplication length is also increasing). This results in the observed 'C' shape of the Paschen curve, i.e., double-valued behavior, at very high $E/n = V/nd$.

4. Summary

We developed a reduced flux-balance quasi-analytical model to investigate ionization breakdown in helium for the applied voltage in the range 10–1000 kV, with corresponding reduced density $nd \sim 1.5 \times 10^{20}\,\mathrm{m}^{-2}$. In our electron/ion/fast neutral model, anisotropic scattering in gas-phase collisions and energy-dependent interactions at the electrode surfaces are carefully taken into account. Three regimes of the breakdown kinetics, labeled 'electron regime', 'ion regime', and 'fast-neutral regime' are identified according to which species contributes the most to the gap-integrated ionization rate. In the fast-neutral regime of particular interest here, the ionization avalanche is directed from the anode towards the cathode. It is initiated by the fast neutral beam backscattered at the cathode, and charge multiplication occurs via multiple successive cycles of ionization and charge exchange. The Paschen curve for helium predicted by the model has been compared to that based on PIC/MCC simulations and to a set of experimental data, both presented in our preceding publication [11]. The Paschen curve predicted by this model is found to be in good agreement with the PIC/MCC result and with experimental data, also reported in [11]. Calculated profiles of particle fluxes in excellent agreement with those obtained in kinetic PIC/MCC simulations. Also, several underlying physical phenomena have been uncovered that are essential in electrical breakdown in an extremely high electric field.

1. The significant role of fast neutral atoms, attributed to backscattering from the cathode and to impact ionization, is demonstrated by the analytical model. Fast-neutral backscattering from the cathode, rather similar in its function of ion-induced secondary electron emission at lower voltage, results in an ion–neutral avalanche, a self-organization mechanism which sustains the discharge current.

2. Stripping loss of fast neutrals, which is the primary loss channel under the condition of strongly anisotropic scattering in gas-phase collisions, has been proven essential to obtain a good agreement with experimental and PIC/MCC results. This is an indirect validation of the model, which assumes velocity distributions strongly peaked in the direction of the electric field.

3. Lastly, the turning-point phenomenon, i.e., the double-valued behavior of the Paschen currve, seen in the PIC/MCC model [11], is also predicted by the present analytical model. The nature of the turning point is that at extremely high values of reduced electric field *E/n* heavy species velocity distributions undergo a transition to runaway regime. This behavior is accounted for in the charge-transfer reaction rate of the reduced model. The turning point occurs primarily because the charge-transfer cross section decreases with increasing projectile energy. The effect is amplified by the decrease in the fast-neutral flux reflection coefficient at high *E/n*.

Acknowledgments

Appendix A. Rate coefficients for helium

In this appendix, we address energy-dependent values and corresponding integrated rates (reaction coefficients) for the cross sections, secondary electron yields, and surface back-scattering yields for ions and fast neutrals for discharge in helium in extremely high electric fields. The same data on cross sections, electron yields, and reflection coefficients as adopted in [11] are used presently in order to make a valid comparison between the analytical and PIC/MCC kinetic models. The electron-impact ionization rate was discussed in the main text and will not be considered in this appendix. In what follows, the values of reaction coefficients α_x/n are in units of $10^{-20}\,\mathrm{m}^2$, cross sections Q_x are in $10^{-20}\,\mathrm{m}^2$, and particle energies ε and effective ion temperature T_i are in eV, unless noted otherwise. The coefficients given below depend on *E/n* through the effective ion temperature T_i parameterizing velocity distribution, approximated with a one-dimensional half-Maxwellian. The relation between T_i and *E/n* is given by equation (7) in the main text.

A.1. Reaction coefficients for energetic ions

Approximate formula for charge exchange cross section can be expressed as $Q_{ct}(\varepsilon) = (5.282 - 0.294 \ln \varepsilon)^2$, based on which the charge exchange coefficient, obtained by flux-averaging over the ion distribution, can be in turn approximated as

$$\frac{\alpha_{ct}}{n}(T_i) = (5.282 - 0.294 \ln T_i)^2 + 0.171 + 0.339 \times (5.282 - 0.294 \ln T_i). \tag{A1}$$

For ion-impact ionization, we utilize the following analytic fit for the cross-section data (valid for projectile energies up to 60 keV):

$$Q_{ii}(\varepsilon) = 0.252 + 1.099 \times 10^3 \sqrt{\varepsilon}/(\varepsilon + 4.650 \times 10^5). \tag{A2}$$

Therefore the corresponding reaction coefficient is obtained by flux-averaging the ionization cross section over the ion distribution. An analytical fit can be provided in the following form:

$$\frac{\alpha_{ii}}{n}(T_i) = \frac{10^{-4}}{T_i}[2.516 \times 10^{-17}T_i + 1.099 \times 10^{-13} \times \sqrt{\pi T_i} - 2353.172 \times A'(a)] \tag{A3}$$

where $A'(a) = \chi(a - 100) \times (1 - 1/2a)/\sqrt{a\pi} + \chi(100 - a)$ erf$(\sqrt{a})\exp[a\chi(100 - a)]$, χ is the step function, erf is the error function, and $a = 4.650 \times 10^5/T_i$. Note that $\frac{\alpha_{ii}}{n}$ in equation (A3) is in units of m^2.

A.2. Fast neutral atom reaction coefficients

A.2.1. Primary fast-atom-neutral ionization coefficient. For primary fast atoms produced in charge exchange collisions, the ionization coefficient is expressed by equation (11) in the main text. To evaluate this expression, we first approximate the product of ionization cross section $Q_{ai}(\varepsilon)$ and charge exchange cross section $Q_{ct}(\varepsilon)$ as follows:

$$Q_{ct}(\varepsilon)Q_{ai}(\varepsilon) = 30.6685(\varepsilon/60842)/(\varepsilon/60842 + 1)^2, \tag{A4}$$

which is in units of $10^{-40}\,\mathrm{m}^4$ and valid for projectile (laboratory frame) energies up to 80 KeV. The following approximation can be given for the resulting value of $\frac{\alpha_{ai}}{n}(T_i)$ in equation (11):

$$\frac{\alpha_{ai}}{n}(T_i) = 30.6685b[(1 + b)B'(b) - 1]/\frac{\alpha_{ct}}{n} \tag{A5}$$

where $b = 60\,842/T_i$ and

$$B'[b(T_i)] = \exp[b\chi(1 - b)]\chi(b)\chi(1 - b)C'(b) + \chi(b - 1)D'(b)/b,$$

$$
C^{'}[b(T_i)] = -0.577 + b\{1 + b\{-0.250 + b
$$
$$
\times[0.055 + b(-0.010 + b0.001)]\}\} - \ln(b),
$$

$$
D^{'}[b(T_i)]
$$
$$
= \frac{\{0.268 + b\{8.635 + b[18.059 + b(8.573 + b)]\}\}}{\{3.958 + b\{21.1 + b[25.633 + b(9.573 + b)]\}\}}.
$$

A.2.2. Ionization coefficient for backscattered fast neutrals.
Equation (13) in the main text gives an expression for the ionization coefficient due to fast neutrals backscattered from the cathode and traveling towards the anode. The denominator on the right-hand side (first term) can be approximated as

$$
\delta_2(T_i) = \{[3.7 - 0.315\ln(T_i)]^2 + 0.196 + 0.364
$$
$$
\times[3.7 - 0.315\ln(T_i)]\}T_i \qquad (A6)
$$

and the numerator as

$$
\delta_1(T_i) = 21550.225\{-c\{[-1 + B^{'}(c)c] + B^{'}(c)\}\} + 1 - B^{'}(c)c,
$$
$$
\qquad (A7)
$$

where $c(T_i) = 16\,641.1/T_i$ and the function $B^{'}$ is the same as entering equation (5A). Hence equation (13) yields

$$
\frac{\alpha_{bi}}{n}(T_i) = \frac{\delta_1}{\delta_2}1.5. \qquad (A8)
$$

A.2.3. Secondary electron yields and fast-atom backscattering coefficient.
An analytical fit of the same form as developed in [14] for argon is used to approximate secondary electron yields of ions and of fast neutrals at the cathode. The fitting functions for SEE yields by ions and by fast atoms work quite well for projectile energies up to 10^6 eV. When averaged over the ion distribution $\exp(-\varepsilon/T_i)$, the electron emission yield by ions is approximated as

$$
\gamma_i(T_i) = 0.3 + 1.55\,(T_i/1000)^{1.9}/[1 + (T_i/600)^{1.54}]. \quad (A9)
$$

Likewise, by averaging over the resulting energy distribution of fast helium atoms produced in charge exchange collisions, the fast-atom induced electron emission yield is given by

$$
\gamma_a(T_i) = 310^{-5}(0.75T_i)^{1.8}\exp(-622.5/T_i)/
$$
$$
\times\ [1 + (T_i/400)^{1.56}]. \qquad (A10)
$$

Regarding the flux-averaged backscattering coefficient R_a of fast atoms at the cathode, based on the analytical fit for energy-dependent reflection yield given by equation (23) in

[11] (which is valid below 100 KeV), it is convenient to convert equation (14) into the following form:

$$
R_a(T_i) = \frac{\delta_2}{T_i}\bigg/\frac{\alpha_{cx}}{n}. \qquad (A11)
$$

We note that the ion reflection (which occurs with neutralization) is neglected, owing to the ion flux collected at the cathode being much smaller than that of fast neutrals. Their ratio scales as d/λ_{cx}.

Appendix B. Solution for the structure of the discharge

In this section, we present the solution to the set of linear equations comprising the present model of steady-state Townsend discharge (refer to model 4 in table 1). It is given by the electron flux $\Gamma_e(x)$, the ion flux $\Gamma_i(x)$, the primary fast-atom flux $\Gamma_a(x)$, and the reflected-fast-atom flux $\Gamma_b(x)$. According to equations (3), (5), (10), and (12) with boundary conditions (8), (9) and (15), we find the particle fluxes (normalized to $\Gamma_t = \Gamma_e + \Gamma_i$) as follows:

$$
\Gamma_e(x)/\Gamma_t = \Bigg\{ \frac{[-NR_a/U_3 + (\beta + QR_a)U_2/U_1 - S]}{MR_a}\exp(\lambda_1 x)
$$
$$
+ \frac{1}{U_3}\exp(\lambda_2 x) - \frac{U_2}{U_1}\exp(\lambda_3 x) + 1\Bigg\}/(1 - P),
$$
$$
\qquad (B1)
$$

$$
\Gamma_i(x)/\Gamma_t = 1 - \Gamma_e(x)/\Gamma_t, \qquad (B2)
$$

$$
\Gamma_a(x)/\Gamma_t = \Bigg\{ -\frac{(-NR_a/U_3 + (\beta + QR_a)U_2/U_1 - S)}{R_a}\exp(\lambda_1 x)
$$
$$
- \frac{N}{U_3}\exp(\lambda_2 x) + \frac{U_2}{U_1}Q\exp(\lambda_3 x) - S\Bigg\}/(1 - P),
$$
$$
\qquad (B3)
$$

$$
\Gamma_b(x)/\Gamma_t = -\frac{U_2}{U_1}\beta\exp(\lambda_3 x)/(1 - P), \qquad (B4)
$$

where the functions M, N, Q, S, P, and β are those entering equation (16) in the main text, and

$$
U_1 = [\exp(\lambda_3 d) - \exp(\lambda_1 d)(\beta + QR_a)/MR_a]
$$
$$
- \left[\frac{\exp(\lambda_2 d) - \exp(\lambda_1 d)N/M}{(1 + \gamma_i + N\gamma_a) - (1 + \gamma_i + M\gamma_a)N/M}\right]
$$
$$
\times[(1 + \gamma_i + Q\gamma_a) - (1 + \gamma_i + M\gamma_a)(\beta + QR_a)/MR_a],
$$

$$
U_2 = [P - \exp(\lambda_1 d)S/MR_a]
$$
$$
- \left[\frac{\exp(\lambda_2 d) - \exp(\lambda_1 d)N/M}{(1 + \gamma_i + N\gamma_a) - (1 + \gamma_i + M\gamma_a)N/M}\right]
$$
$$
\times[(1 + P\gamma_i + S\gamma_a) - (1 + \gamma_i + M\gamma_a)S/MR_a].
$$

$$
U_3 = \frac{(1 + \gamma_i + N\gamma_a) - (1 + \gamma_i + M\gamma_a)N/M}{\{[(1 + \gamma_i + Q\gamma_a) - (1 + \gamma_i + M\gamma_a)(\beta + QR_a)/MR_a]U_2/U_1 - [(1 + P\gamma_i + S\gamma_a) - (1 + \gamma_i + M\gamma_a)S/MR_a]\}}
$$

Alongside the full analytical model formulated above, the following three truncated models in table 1 are introduced to aid in the discussion.

B.1. Reduced model for electron regime (model 1): $\alpha_{ii} = \alpha_{ai} = \gamma_a = R_a = 0$

These assumptions bring the original Townsend electron-multiplication model

$$\frac{d\Gamma_{e,1}(x)}{dx} = \alpha_{ei}(E, n)\Gamma_{e,1}(x). \tag{B5}$$

The boundary condition involves ion-induced electron emission from the cathode:

$$\Gamma_{e,1}(0) = \gamma_i\Gamma_{i,1}(0) = \gamma_i[\Gamma_t - \Gamma_{e,1}(0)]. \tag{B6}$$

Therefore, normalized electron and ion fluxes write as

$$\frac{\Gamma_{e,1}(x)}{\Gamma_t} = \frac{\gamma_i}{\gamma_i + 1}\exp(\alpha_{ei}x), \tag{B7}$$

$$\frac{\Gamma_{i,1}(x)}{\Gamma_t} = 1 - \frac{\Gamma_{e,1}(x)}{\Gamma_t}. \tag{B8}$$

B.2. Second reduced model for ion regime (model 2): $\alpha_{ai} = \gamma_a = R_a = 0$

Under this condition, the model simplifies as

$$\frac{d\Gamma_{e,2}(x)}{dx} = -\frac{d\Gamma_{i,2}(x)}{dx} = \alpha_{ei}(E, n)\Gamma_{e,2}(x) + \alpha_{ii}(E/n)\Gamma_{i,2}(x), \tag{B9}$$

with the same boundary condition equation (B6). The solution for electron and ion fluxes is

$$\frac{\Gamma_{e,2}(x)}{\Gamma_t} = \left\{-\frac{1 + \gamma_i\alpha_{ei}/\alpha_{ii}}{1 + \gamma_i}\exp[(\alpha_{ei} - \alpha_{ii})x] + 1\right\}\bigg/$$
$$(1 - \alpha_{ei}/\alpha_{ii}), \tag{B10}$$

$$\frac{\Gamma_{i,2}(x)}{\Gamma_t} = 1 - \frac{\Gamma_{e,2}(x)}{\Gamma_t}. \tag{B11}$$

B.3. Third reduced model for fast-neutral regime (model 3): $R_a = 0$

In the third model, equations (3), (5) and (10) reduce to the following expressions:

$$-\frac{d\Gamma_{i,3}}{dx} = \frac{d\Gamma_{e,3}}{dx} = \alpha_{ei}\Gamma_{e,3} + \alpha_{ii}\Gamma_{i,3} + \alpha_{ai}\Gamma_{a,3}, \tag{B12}$$

$$\frac{d\Gamma_{a,3}}{dx} = -\alpha_{ct}\Gamma_{i,3}, \tag{B13}$$

with the boundary condition given by equation (8) in the main text:

$$\Gamma_{e,3}(0) = \gamma_i\Gamma_{i,3}(0) + \gamma_f\Gamma_{a,3}(0) \tag{B14}$$

$$\Gamma_{i,3}(d) = 0. \tag{B15}$$

Therefore we obtain the solution for the fluxes:

$$\frac{\Gamma_{e,3}(x)}{\Gamma_t} = \frac{-\exp[(\lambda_2 - \lambda_1)d][1 + \gamma_a\alpha_{ei}/\alpha_{ai}]}{\{(1 + \gamma_i)\{\exp[(\lambda_2 - \lambda_1)d] - 1\}\}}\exp(\lambda_1 x)$$
$$+ \frac{[1 + \gamma_a\alpha_{ei}/\alpha_{ai}]}{\{(1 + \gamma_i)\{\exp[(\lambda_2 - \lambda_1)d] - 1\}\}}\exp(\lambda_2 x) + 1 \tag{B16}$$

$$\frac{\Gamma_{i,3}(x)}{\Gamma_t} = 1 - \frac{\Gamma_{e,3}(x)}{\Gamma_t}. \tag{B17}$$

ORCID iDs

Liang Xu https://orcid.org/0000-0002-8729-1984
Timothy J Sommerer https://orcid.org/0000-0001-7946-2870

References

[1] Townsend J S 1915 *Electricity in Gases* (Oxford: Clarendon)
[2] Lieberman M A and Lichtenberg A J 1994 *Principles of Plasma Discharges and Materials Processing* (New York: Wiley)
[3] McClure G W 1961 *Phys. Rev.* **124** 969
[4] McClure G W and Granzow K D 1962 *Phys. Rev.* **125** 3
[5] Bhasavanich D and Parker A 1977 *Proc. R. Soc.* A **358** 385
[6] Lauer E J, Yu S S and Cox D M 1981 *Phys. Rev.* A **23** 2250
[7] Hillmann H, Muller F and Wenz H 1994 *Plasma Sources Sci. Technol.* **3** 496
[8] Donkó Z 2001 *Phys. Rev.* E **64** 26401
[9] Hartmann P, Donko Z, Bano G, Szalai L and Rozsa K 2000 *Plasma Sources Sci. Technol.* **9** 183
[10] Macheret S O and Shneider M N 2013 *Phys. Plasmas* **20** 101608
[11] Xu L, Khrabrov A V, Kaganovich I D and Sommerer T J 2017 *Phys. Plasmas* **24** 093511
[12] Druyvesteyn M J and Penning F M 1940 *Rev. Mod. Phys.* **12** 87
[13] Hayashi M 1982 *J. Phys. D: Appl. Phys.* **15** 1411
[14] Fletcher J 1985 *J. Phys. D: Appl. Phys.* **18** 221
[15] Bhatnagar P L, Gross E P and Krook M 1954 *Phys. Rev.* **94** 511
[16] Jelenković B M and Phelps A V 2005 *Phys. Rev.* E **71** 016410
[17] Phelps A V and Lj Pterovic Z 1999 *Plasma Sources Sci. Technol.* **8** R21
[18] Hayashi M 1982 *J. Phys. D* **15** 1411
[19] Phelps A V and Jelenković B M 1988 *Phys. Rev.* A **38** 2975
[20] Granzow K D and McClure G W 1962 *Phys. Rev.* **125** 1792
[21] Pace J D and Parker A B 1973 *J. Phys. D: Appl. Phys.* **6** 1525
[22] Adams S F *et al* 2017 *J. Phys.: Conf. Series* **927** 012001
[23] Phelps A V, Jelenković B M and Pitchford L C 1987 *Phys. Rev.* A **36** 5327
[24] Parker A B and Johnson P C 1971 *Proc. R. Soc. London, Ser.* A **325** 511
[25] Darlington E H 1975 *J. Phys. D: Appl. Phys.* **8** 85
[26] Lawler J E 1985 *Phys. Rev.* A **32** 2977
[27] Loveless A M and Garner A L 2017 *Phys. Plasmas* **24** 113522
[28] Phelps A V 2002 *Bull. Am. Phys. Soc.* **47** 41
[29] Guseva L G 1964 On discharge striking in polyatomic gases at pd < (pd)min *Investigations into Electrical Discharges in Gases* ed B N Klyarfel'd (New York: Elsevier) pp 1–11